COMMUNICATION

In situ synergistic halogen passivation of semiconducting PbS quantum dot inks for efficient photovoltaics†

Xiaobo Ding,‡[a,b] Xin Wen,‡[a] Yuto Kawata,[c] Yang Liu,[a] Guozheng Shi,[a,c] Refka ben Ghazi,[a] Xiang Sun,[a] Yujie Zhu,[a] Hao Wu,[a] Haotian Gao,[a] Qing Shen, [ID][c] Zeke Liu [ID] *[a,b] and Wanli Ma [ID] [a,b]

Lead sulfide colloidal quantum dots (PbS CQDs) show great potential in next-generation photovoltaics. However, their high specific surface area and complex surface crystallography lead to a high surface trap density, which normally requires more than one type of capping ion or ligand to achieve effective surface passivation. In this study, we performed *in situ* mixed halogen passivation (MHP) during the direct synthesis of semiconducting PbS CQD inks by using different lead halogens. The different halogens can bind with the surface of the CQD throughout the nucleation/growth process, resulting in optimal surface configuration. As a result, the MHP CQD exhibited superior surface passivation compared to the conventionally iodine-capped CQDs. Finally, we achieved a substantial improvement in efficiency from 10.64% to 12.58% after the MHP treatment. Our work demonstrates the advantages of exploring efficient passivation in the directly synthesized CQD inks.

[a]*Institute of Functional Nano & Soft Materials (FUNSOM), Joint International Research Laboratory of Carbon-Based Functional Materials and Devices, Soochow University, Suzhou, 215123 Jiangsu, PR China. E-mail: zkliu@suda.edu.cn*
[b]*Jiangsu Key Laboratory of Advanced Negative Carbon Technologies, Soochow University, Suzhou, 215123 Jiangsu, PR China*
[c]*Faculty of Informatics and Engineering, The University of Electro-Communications, Tokyo 182-8585, Japan*
†Electronic supplementary information (ESI) available. See DOI: https://doi.org/10.1039/d3nr05951k
‡These authors contributed equally to this work.
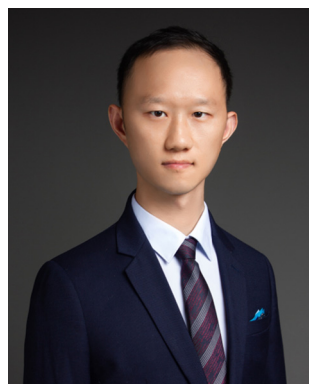
Zeke Liu is an associate professor at Soochow University. He obtained his PhD degree from Soochow University, and worked as a joint PhD student at the University of California, Berkeley and Lawrence Berkeley National Laboratory. Before he joined Soochow University in 2019, he worked as a joint postdoctoral scholar in Indiana University, Bloomington and Soochow University. His current research interests are focused on the design and synthesis of semiconductor quantum dots/nanocrystals and their application in optoelectronic devices.

Zeke Liu

1. Introduction

PbS colloidal quantum dots (CQDs) have attracted substantial attention for use in photovoltaic devices due to their long-term stability,[1,2] broad absorption spectra[3–5] and enticing multi-exciton generation.[6,7] They have been classified as one of the three primary solution-processed photovoltaic materials, along with organic semiconductors and metal halide perovskites.[8,9] The nanoscale size of CQD materials results in a high surface area/volume ratio, leading to numerous surface dangling bonds and trap states. The management of these surface traps is critical to the achievement of high photovoltaic performance and has been the primary research focus in the field of CQD solar cells.[10–15] In the early stage, bidentate thiol molecules (ethanedithiol, benzenedithiol, and 3-mercaptopropionic acid) were widely employed to passivate PbS CQDs due to the strong binding affinity between thiol and surface Pb.[16–20] To further increase the coupling between the CQDs, inorganic halogen ions (especially iodide) have been explored as efficient ligands that exhibit excellent passivation on the surface of PbS CQDs.[1,21–26] Additionally, the sole ligand typically cannot fully passivate the entire surface of PbS CQDs due to steric hindrance. Therefore, additional ions (such as Br-, Cl-, SCN-) or molecules (such as thiols) have been introduced to enhance surface passivation.[27–32]

Until now, PbS CQD passivation has been implemented through a process known as ligand exchange. In the process, the short ions or ligands were employed to substitute the original long-chain ligands (*e.g.*, oleate), which is the essential step for ensuring sufficient charge transport in the CQD film for optoelectronic devices.[33–36] Ideally, all the Pb–oleate bonds

should be broken and then the surface Pb should form new bonds with incoming short ions or ligands. However, due to the steric hindrance of incoming ligands and inconsistent ligand exchanges, it is challenging for the incoming ions or short ligands to bind with all the uncoordinated sites generated after the break-up of the Pb–oleate bonds, inevitably resulting in the formation of trap states.[37,38] This issue is even more prominent when using multiple components in the ligand exchange toward synergistic passivation, as the reactivity and steric hindrance of each passivator is hard to be well coordinated.[34]

Recently, we have investigated a novel strategy for the direct synthesis of semiconducting PbS CQD inks.[38–40] This method completely circumvents the problematic ligand exchange process and the resulting PbS CQDs are directly passivated with iodide. This strategy provides a new platform to effectively design multiple passivations during the CQD synthesis and straightforwardly deliver outstanding passivation to the final optoelectronic application. Taking advantage of the advanced direct-synthesis CQD ink protocol, in this study, we developed an *in situ* mixed halogen passivation (MHP) strategy by introducing different lead halogens as precursors during CQD ink synthesis. As halogens are involved in the entire CQD nucleation/growth processes and dynamically interact with the CQD surface, they attach to the surface with the most favorable thermodynamic configuration. The resulting MHP CQDs exhibit improved surface halogen coverage, advanced surface passivation, and fewer trap states than the sole iodide-capped

CQDs (Fig. 1a). Finally, the photovoltaic device based on MHP CQD inks achieves a power conversion efficiency (PCE) of 12.58%, which is significantly higher than that of the control device (10.64%) based on sole iodide-capped CQD inks.

2. Experimental

2.1 Direct synthesis of PbS CQD inks

The control PbS CQD inks were synthesized by fully dissolving 6 mmol of PbI_2 and 1 mmol of DPhTA in 9 mL of DMF under a nitrogen atmosphere. Subsequently, 1 mL of BA was rapidly injected into the precursor solution under a 0 °C ice bath, and the reaction mixture was left undisturbed for 10 min. Then, toluene was added as an anti-solvent, followed by centrifugation at 8000 rpm for 5 min. The resulting CQD solids were stored in an N_2 glovebox. For the MHP CQD inks, partial PbI_2 was replaced with $PbBr_2$ or $PbCl_2$ prior to the addition of BA. The purification process was the same as that for the control inks.

2.2 Solar cell fabrication

ITO glass was first cleaned sequentially with deionized water, IPA, and acetone in an ultrasonic apparatus, and then treated with UV-ozone for 30 minutes. Subsequently, a solution of ZnO nanoparticles was spin-cast onto the ITO glass at 2500 rpm for 20 seconds. The PbS CQD ink solution (with a concentration of 700 mg mL^{-1}) was then spin-coated at 2000 rpm for
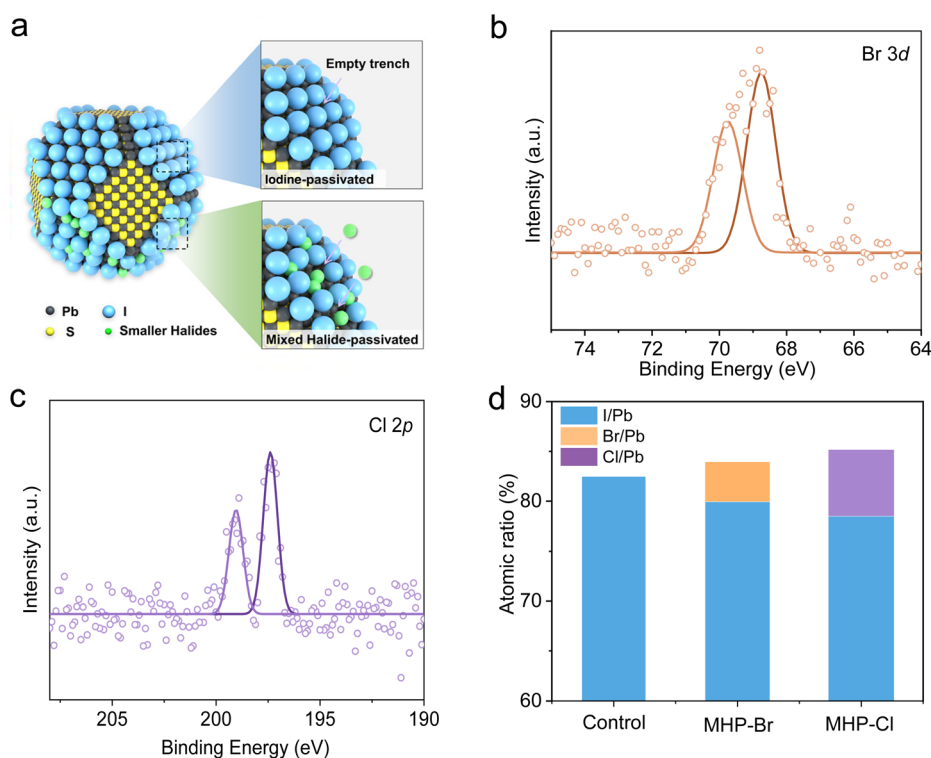

Fig. 1 (a) Schematic of the mixed halogen surface passivation (MHP) strategy based on the direct synthesis of PbS CQD inks. (b–c) XPS spectra in Br 3d and Cl 2p regions for MHP-Br and MHP-Cl CQD films. (d) Elemental ratios extracted from the XPS spectra.

40 seconds, and annealed at 70 °C for 10 minutes under an inert atmosphere. For the hole transport layer, 20 mg mL^{-1} oleate-capped PbS CQDs were spin-coated at 2500 rpm for 20 seconds, followed by treatment with a 1,2-ethanedithiol (EDT) solution (with a concentration of 0.04 vol% in acetonitrile) for 30 seconds and rinsing twice with acetonitrile. This process was repeated twice to achieve a thickness of approximately 40 nm. The prepared devices were stored under dry air overnight for further oxidation. Finally, a 100 nm Au layer was evaporated through thermal evaporation at a rate of 0.5 Ås^{-1} under a high vacuum of less than 1×10^{-5} mbar through a shadow mask to define a total active area of 0.0725 cm^2. The devices were stored under ambient air (with a relative humidity of approximately 30%) for the air stability test. The procedures for the synthesis of ZnO nanoparticles and oleate-capped PbS CQDs are presented in the ESI.†

2.3 Measurements and characterization

X-ray photoelectron spectroscopy (XPS) was carried out in an ultrahigh vacuum (UHV) system with a base pressure of 1.0×10^{-10} mbar and tested with a monochromatized Al Kα light source (1486.75 eV). The absorbance spectra were recorded on PerkinElmer model Lambda 750. The photoluminescence spectra and photoluminescence decays of CQD solutions were recorded on a FluoroMax-4 spectrofluorometer (HORIBA Scientific). The photoluminescence spectra of QD films were measured on an Applied NanoFluorescence spectrometer (USA) by using an excitation laser source of 785 nm. The photoluminescence quantum yields (PLQY) of the CQD solutions were recorded using an integration sphere incorporated into the FLS980 spectrometer. The device cross-sectional images were characterized by SEM on a Zeiss Supra 55 field. Current–voltage I–V characteristics were recorded using a Keithley 2400 digital source meter under simulated AM 1.5G solar irradiation at 100 mW cm^{-2} (Newport, Class AAA solar simulator, 94023A-U). The light intensity is calibrated using a certified Oriel reference cell (91150 V) and verified with an NREL-calibrated Hamamatsu S1787–04 diode.

3. Results and discussion

The control PbS CQD inks were synthesized following our previous report.[39] Briefly, PbI$_2$ and diphenyl thiourea (DPhTA) were dissolved in N,N-dimethylformamide (DMF), serving as the Pb and S precursors respectively. Butylamine (BA) was then injected into the solution to initiate the reaction. In the mixed halogen passivation (MHP) strategy, partial PbI$_2$ was replaced with PbBr$_2$ (MHP-Br) or PbCl$_2$ (MHP-Cl). X-ray photoelectron spectroscopy (XPS) was first performed to characterize the impact of MHP on CQD surface chemistry. As shown in Fig. 1b and c, well-defined Br 3d and Cl 2p peaks can be observed for MHP-Br and MHP-Cl samples, respectively. The energy dispersive spectroscopy (EDS) mapping conducted under the scanning electron microscope (SEM) also reveals the uniform distribution of Br and Cl for the corresponding CQD films

(Fig. S1†). The XPS and SEM-EDS results collectively indicate that Br$^-$ or Cl$^-$ ions have been effectively incorporated into the CQD surface using the MHP strategy. We further calculated the detailed elemental ratios for the MHP samples by integrating the areas of the XPS spectra peaks of I 3d and Pb 4f (Fig. S2†). The extracted elemental ratios are summarized in Fig. 1d. The Br/Pb ratio in MHP-Br and Cl/Pb ratio in MHP-Cl are 4.01% and 6.69%, respectively. Meanwhile, the I/Pb ratio decreased from 82.48% (control) to 79.94% (MHP-Br) and 78.49% (MHP-Cl). More importantly, it was observed that the (Br + I)/Pb and (Cl + I)/Pb ratios can reach 83.95% for MHP-Br and 85.18% for MHP-Cl samples, respectively. The above results imply that the MHP can achieve a higher halogen coverage due to the smaller sizes of the Br$^-$ and Cl$^-$ ions, which can bind to the uncoordinated Pb sites that are inaccessible to much larger I$^-$ ions. Previous reports have suggested that higher surface halogen coverage may help reduce surface trap states.[23,37]

Additional optical characterization was further carried out to study the effect of the MHP strategy. As depicted in Fig. 2a, the MHP-Br and MHP-Cl CQD solutions exhibit only a slight shift towards shorter wavelengths on the absorption edge, likely attributed to the modified reaction kinetics following the incorporation of different Pb precursors. However, the MHP CQDs demonstrate significantly enhanced photoluminescence (PL) intensities. The PL quantum yields (PLQY) were estimated to be 9.53%, 12.78% and 17.42% for control, MHP-Br and MHP-Cl QDs respectively (Fig. S3†). Meanwhile, the average PL lifetime also improved from 1.10 μs for the control CQD solution to 1.54 μs (MHP-Br) and 2.21 μs (MHP-Cl) (Fig. 2b and Table S1†). The marked increase in the PLQY and PL lifetime indicates that the nonradiative trap states have been efficiently suppressed (Fig. 2c).[38] Furthermore, the optical behaviors of the CQD solid film were studied. As shown in Fig. 2d, the absorption edges of the MPH CQD films exhibit a redshift compared to that of the control, indicating that the MPH CQD films display an improved inter-dot coupling.[41,42] The PL intensity and PL lifetime of the CQD films exhibit a reversed trend compared to those in solution (Fig. 2d, e and Table S2†), which can be attributed to the rapid charge transfer within the strongly electronically coupled MHP QD films. The space-charge-limited current (SCLC) measurement was then performed to evaluate the trap density and carrier mobility. As shown in Fig. 2f, the SCLC of the electron-only devices (ITO/ZnO/PbS-film/ZnO/Ag) can be defined as the ohmic region, trap-filling region, and trap-free region. The torsion voltage at the critical point between the ohmic region and the trap filling region is defined as the trap filling limit voltage (V_{TFL}), which can be used to determine the trap state concentration (Fig. 2d).[43] MHP-Cl CQDs exhibited the lowest electron trap density (1.91×10^{16} cm^{-3}), followed by MHP-Br (2.37×10^{16} cm^{-3}) and control (2.57×10^{16} cm^{-3}). Electron mobility is a metric to evaluate electron transport ability. The calculated electron mobilities are 1.65×10^{-6} cm^2 V^{-1} s^{-1}, 2.47×10^{-6} cm^2 V^{-1} s^{-1} and 3.61×10^{-6} cm^2 V^{-1} s^{-1} for control, MHP-Br and MHP-Cl CQDs films, respectively (Fig. S4†). These results
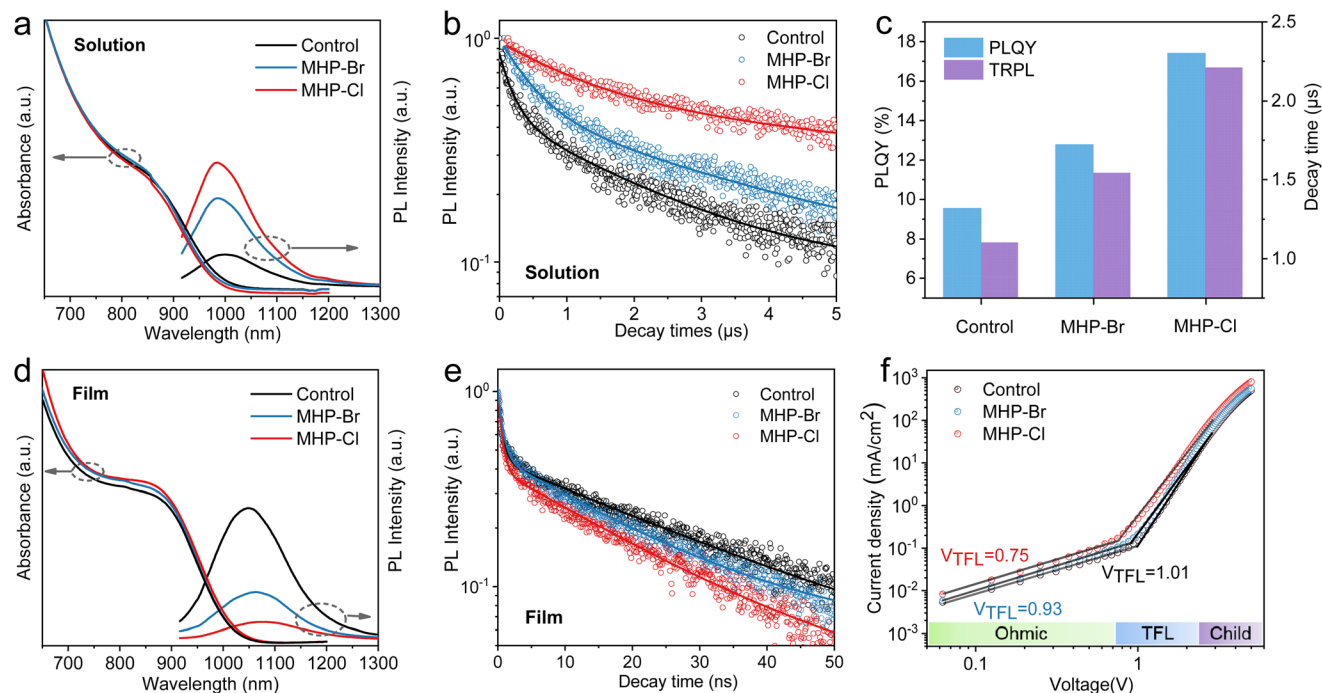
Fig. 2 (a) Absorbance and steady-state PL spectra of PbS CQD solutions. (b) TRPL of the CQD inks. (c) PLQY and TRPL results of the CQD solutions. (d) Absorbance and steady-state PL spectra of the CQD solid films. (e) TRPL of the CQD films. (f) Space charge limited current (SCLC) measurements for the CQD films.

indicate that the MHP strategy can enhance surface passivation of the PbS QD and promote inter-dot coupling, which is beneficial for photovoltaic applications.

The directly synthesized QD inks were then applied as an active layer for solar cell fabrication. Fig. 3a shows the schematic illustration of the device structure (ITO/ZnO/PbS-inks/PbS-EDT (1,2-ethanedithiol)/Au), where ZnO and PbS-EDT serve as electron and hole transport layers, respectively.[1,39] Fig. 3b and Fig. S5† display a cross-sectional SEM image of a typical device. The halogen input ratios used during the CQD synthesis were optimized first, and the results indicate that the best power conversion efficiencies (PCEs) were obtained at $PbBr_2/PbI_2 = 5\%$ and $PbCl_2/PbI_2 = 10\%$ (molar ratio), respectively. (Tables S3 and S4†) The PCE histograms of the devices are shown in Fig. S6.† The MHP-Cl device exhibits champion PCE up to 12.58%, with an open-circuit voltage (V_{oc}) of 0.66 V, a short-circuit current density (J_{sc}) of 27.73 mA cm^{-2}, and a fill factor (FF) of 68.78%. The current–voltage (J–V) curves for the champion control, MHP-Br and MHP-Cl devices are shown in Fig. 3c. Compared with the control device (PCE = 10.64%, with a V_{oc} of 0.64 V, J_{sc} of 26.63 mA cm^{-2}, FF of 62.45%), the improvement of PCE in the MHP device is primarily due to the increase in V_{oc} and FF, which correspond to the improved passivation of the MHP strategy. Additionally, J_{sc} calculated from EQE integration shows good agreement with the values obtained from the J–V measurement, as depicted in Fig. 3d. The J–V scans conducted in both forward and reverse directions show similar performance, indicating minimal hysteresis in the devices (Fig. S7†). Finally, all devices demonstrate excel-

lent storage stability, retaining about 95% of their initial PCE after storage in an ambient atmosphere (RH 30%) for over 800 hours (Fig. S8†).

Finally, we characterized the control and MHP solar cells to comprehend the kinetics responsible for the improved photovoltaic performance. The Nyquist plots of the control and MHP devices are presented in Fig. 4a. The related parameters are listed in Table S5.† The MHP-Cl device exhibits a lower series resistance ($R_s = 15.25\ \Omega$) than the MHP-Br device ($R_s = 29.08\ \Omega$) and the control device ($R_s = 61.72\ \Omega$). The results suggest that the MHP device has improved charge carrier transport and suppressed charge carrier recombination compared to the control device, consistent with improved V_{oc} and FF values. Furthermore, the Mott–Schottky analysis of the capacitance–voltage (C–V) curves was conducted to examine the built-in potential (V_{bi}) of the control and MHP solar cells (Fig. 4b). The MHP-Cl device exhibits a V_{bi} value of 0.57 V, which is higher than that of the MHP-Br device (V_{bi} 0.54 V) and the control device (V_{bi} 0.52 V), indicating a broader depletion layer that promotes charge transport and accelerates charge carrier separation.[44] We also carried out C–V tests under different frequencies. As illustrated in Fig. 4c and Fig. S9,† the MHP-Cl devices show higher built-in potential than both the MHP-Br and control devices. The larger V_{bi} in the MHP-Cl device indicates a stronger built-in field, corresponding to the improved V_{oc} and FF in the solar cell devices. Meanwhile, photovoltage decay spectra measurements were performed on both devices (Fig. 4d). The MHP-Cl device shows the longest photovoltage decay time (76.84 µs) compared to
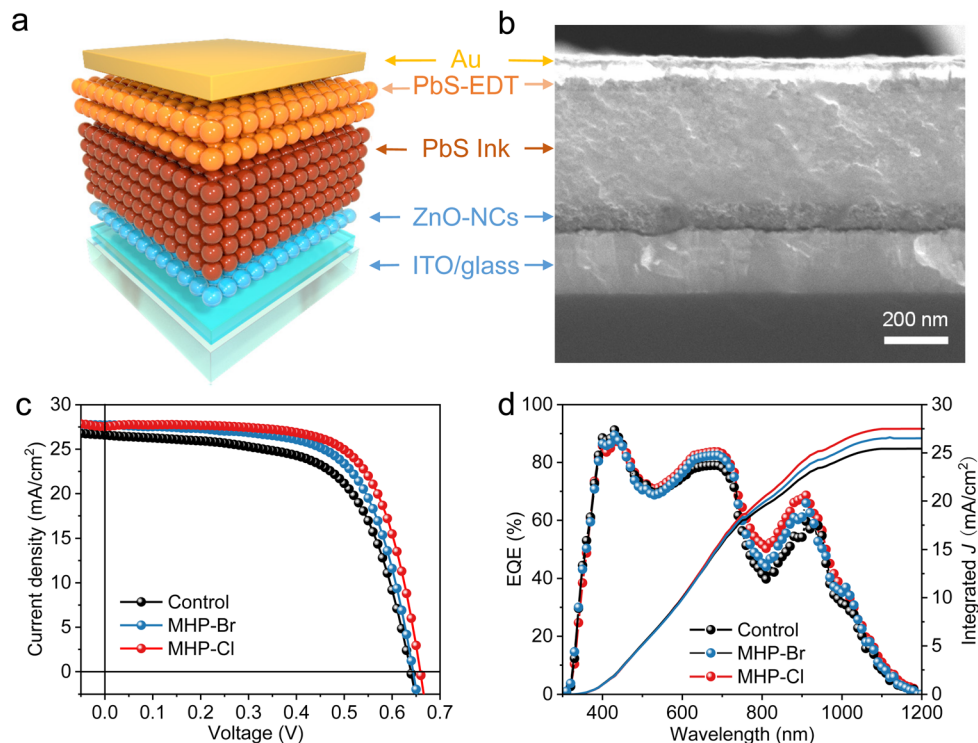
Fig. 3 (a) Schematic illustration of the CQD photovoltaic device. (b) Cross-section SEM image of the PbS CQD photovoltaic device used in this study. (c) *J–V* curves of CQD solar cells obtained under an AM 1.5G solar simulator. (d) EQE curves and integrated JSC of the best devices.
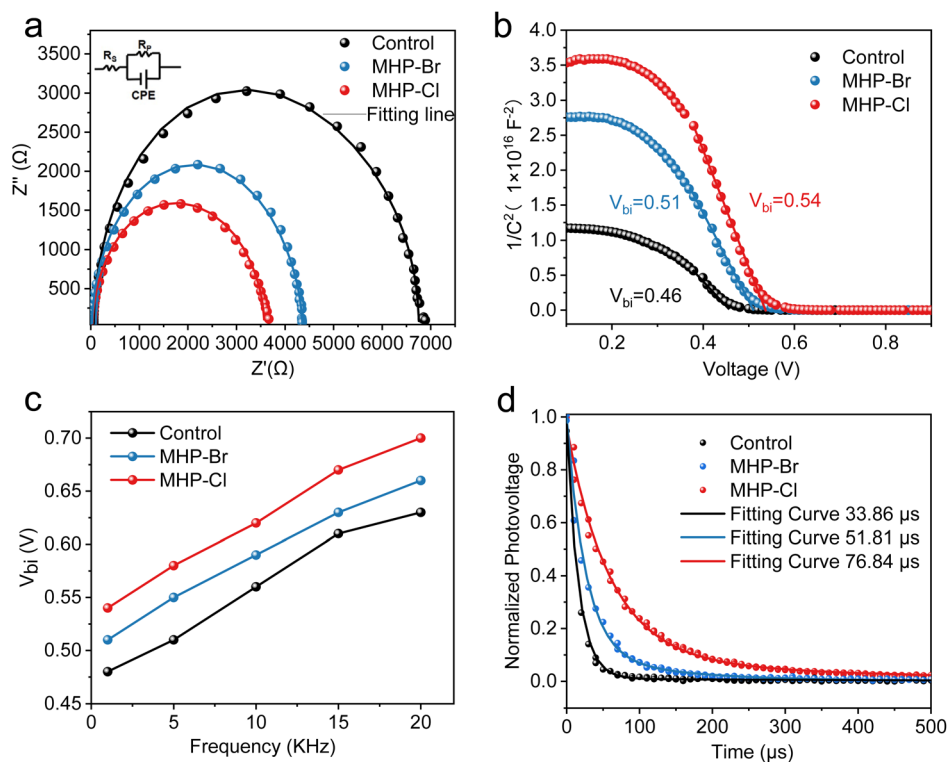

Fig. 4 (a) Nyquist plots (inserted picture is the equivalent circuit model). (b) The Mott–Schottky plot of capacitance *versus* voltage measured under 1 kHz. (c) The extracted V_{bi} values of the CQD devices under different frequencies. (d) Photovoltage decay spectra of the CQD solar cells.

the MHP-Br (51.81 μs) and control (33.86 μs). A larger photo-voltage decay time suggests that the MHP strategy can reduce trap states, thereby suppressing nonradiated recombination.[43,45]

4. Conclusion

In summary, we propose an effective and simple *in situ* mixed halogen passivation (MHP) strategy in the direct synthesis of PbS CQD inks. This strategy utilizes halogens with different sizes to achieve comprehensive passivation of the CQD surface during the synthesis process. The optimized configuration and improved surface coverage of the halogens result in reduced trap states and increased CQD coupling compared to sole iodide ion passivation. The solar cells based on the MHP CQD achieved champion power conversion efficiency (PCE) of 12.58%, significantly higher than that of the control device (10.64%).

Author contributions

Z. L. conceived the idea and supervised the project. X. D. and X. W. designed the experiments and performed the experiments and data analysis. Y. L. conducted PLQY measurements. Y. K., G. S. conducted the PL lifetime measurement. R. G. and X. S. conducted XPS measurements. Y. Z. optimized the CQD synthesis. H. W. and H. G. conducted device characterization. X. D., Q. S., W. M. and Z. L. contributed to data analysis and co-wrote the manuscript.

Conflicts of interest

The authors declare that they have no known competing financial interests.

Acknowledgements

References

1 C. H. Chuang, P. R. Brown, V. Bulovic and M. G. Bawendi, Improved performance and stability in quantum dot solar cells through band alignment engineering, *Nat. Mater.*, 2014, **13**, 796–801.

2 H. Wang, M. Desbordes, Y. Xiao, T. Kubo, K. Tada, T. Bessho, J. Nakazaki and H. Segawa, Highly Stable Interdigitated PbS Quantum Dot and ZnO Nanowire Solar Cells with an Automatically Embedded Electron-Blocking Layer, *ACS Appl. Energy Mater.*, 2021, **4**, 5918–5926.

3 M. C. Weidman, M. E. Beck, R. S. Hoffman, F. Prins and W. A. Tisdale, Monodisperse, air-stable PbS nanocrystals via precursor stoichiometry control, *ACS Nano*, 2014, **8**, 6363–6371.

4 C. Dong, S. Liu, N. Barange, J. Lee, T. Pardue, X. Yi, S. Yin and F. So, Long-Wavelength Lead Sulfide Quantum Dots Sensing up to 2600 nm for Short-Wavelength Infrared Photodetectors, *ACS Appl. Mater. Interfaces*, 2019, **11**, 44451–44457.

5 Y. Xia, S. Liu, K. Wang, X. Yang, L. Lian, Z. Zhang, J. He, G. Liang, S. Wang, M. Tan, H. Song, D. Zhang, J. Gao, J. Tang, M. C. Beard and J. Zhang, Cation–Exchange Synthesis of Highly Monodisperse PbS Quantum Dots from ZnS Nanorods for Efficient Infrared Solar Cells, *Adv. Funct. Mater.*, 2019, **30**, 1907379.

6 O. E. Semonin, J. M. Luther, S. Choi, H.-Y. Chen, J. Gao, A. J. Nozik and M. C. Beard, Peak External Photocurrent Quantum Efficiency Exceeding 100% via MEG in a Quantum Dot Solar Cell, *Science*, 2011, **334**, 1530–1533.

7 M. C. Beard, J. M. Luther, O. E. Semonin and A. J. Nozik, Third generation photovoltaics based on multiple exciton generation in quantum confined semiconductors, *Acc. Chem. Res.*, 2013, **46**, 1252–1260.

8 O. Voznyy, B. R. Sutherland, A. H. Ip, D. Zhitomirsky and E. H. Sargent, Engineering charge transport by heterostructuring solution-processed semiconductors, *Nat. Rev. Mater.*, 2017, **2**, 17026.

9 F. P. Garcia de Arquer, D. V. Talapin, V. I. Klimov, Y. Arakawa, M. Bayer and E. H. Sargent, Semiconductor quantum dots: Technological progress and future challenges, *Science*, 2021, **373**, eaaz8541.

10 G. H. Carey, A. L. Abdelhady, Z. Ning, S. M. Thon, O. M. Bakr and E. H. Sargent, Colloidal Quantum Dot Solar Cells, *Chem. Rev.*, 2015, **115**, 12732–12763.

11 S. Zheng, J. Chen, E. M. J. Johansson and X. Zhang, PbS Colloidal Quantum Dot Inks for Infrared Solar Cells, *iScience*, 2020, **23**, 101753.

12 Y. Liu, G. Shi, Z. Liu and W. Ma, Toward printable solar cells based on PbX colloidal quantum dot inks, *Nanoscale Horiz.*, 2021, **6**, 8–23.

13 L. Duan, L. Hu, X. Guan, C. H. Lin, D. Chu, S. Huang, X. Liu, J. Yuan and T. Wu, Quantum Dots for Photovoltaics: A Tale of Two Materials, *Adv. Energy Mater.*, 2021, **11**, 2100354.

14 J. Liu, K. Xian, L. Ye and Z. Zhou, Open-Circuit Voltage Loss in Lead Chalcogenide Quantum Dot Solar Cells, *Adv. Mater.*, 2021, **33**, e2008115.

15 Q. Zhao, R. Han, A. R. Marshall, S. Wang, B. M. Wieliczka, J. Ni, J. Zhang, J. Yuan, J. M. Luther, A. Hazarika and G. R. Li, Colloidal Quantum Dot Solar Cells: Progressive Deposition Techniques and Future Prospects on Large-Area Fabrication, *Adv. Mater.*, 2022, **34**, e2107888.

16 G. I. Koleilat, L. Levina, H. Shukla, S. H. Myrskog, S. Hinds, A. G. Pattantyus-Abraham and E. H. Sargent, Efficient, stable infrared photovoltaics based on solution-cast colloidal quantum dots, *ACS Nano*, 2008, **2**, 833–840.

17 J. J. Choi, Y. F. Lim, M. E. B. Santiago-Berrios, M. Oh, B. R. Hyun, L. Sun, A. C. Bartnik, A. Goedhart, G. G. Malliaras and H. D. Abruña, PbSe nanocrystal excitonic solar cells, *Nano Lett.*, 2009, **9**, 3749–3755.

18 W. Ma, J. M. Luther, H. Zheng, Y. Wu and A. P. Alivisatos, Photovoltaic devices employing ternary PbSxSe1-x nanocrystals, *Nano Lett.*, 2009, **9**, 1699–1703.

19 W. Ma, S. L. Swisher, T. Ewers, J. Engel, V. E. Ferry, H. A. Atwater and A. P. Alivisatos, Photovoltaic Performance of Ultrasmall PbSe Quantum Dots, *ACS Nano*, 2011, **5**, 8140–8147.

20 K. S. Jeong, J. Tang, H. Liu, J. Kim, A. W. Schaefer, K. Kemp, L. Levina, X. Wang, S. Hoogland, R. Debnath, L. Brzozowski, E. H. Sargent and J. B. Asbury, Enhanced mobility-lifetime products in PbS colloidal quantum dot photovoltaics, *ACS Nano*, 2012, **6**, 89–99.

21 J. Tang, K. W. Kemp, S. Hoogland, K. S. Jeong, H. Liu, L. Levina, M. Furukawa, X. Wang, R. Debnath, D. Cha, K. W. Chou, A. Fischer, A. Amassian, J. B. Asbury and E. H. Sargent, Colloidal-quantum-dot photovoltaics using atomic-ligand passivation, *Nat. Mater.*, 2011, **10**, 765–771.

22 J. Tang, H. Liu, D. Zhitomirsky, S. Hoogland, X. Wang, M. Furukawa, L. Levina and E. H. Sargent, Quantum junction solar cells, *Nano Lett.*, 2012, **12**, 4889–4894.

23 Z. Ning, O. Voznyy, J. Pan, S. Hoogland, V. Adinolfi, J. Xu, M. Li, A. R. Kirmani, J. P. Sun, J. Minor, K. W. Kemp, H. Dong, L. Rollny, A. Labelle, G. Carey, B. Sutherland, I. Hill, A. Amassian, H. Liu, J. Tang, O. M. Bakr and E. H. Sargent, Air-stable n-type colloidal quantum dot solids, *Nat. Mater.*, 2014, **13**, 822–828.

24 Y. Cao, A. Stavrinadis, T. Lasanta, D. So and G. Konstantatos, The role of surface passivation for efficient and photostable PbS quantum dot solar cells, *Nat. Energy*, 2016, **1**, 16035.

25 D. Jia, J. Chen, S. Zheng, D. Phuyal, M. Yu, L. Tian, J. Liu, O. Karis, H. Rensmo, E. M. J. Johansson and X. Zhang, Highly Stabilized Quantum Dot Ink for Efficient Infrared Light Absorbing Solar Cells, *Adv. Energy Mater.*, 2019, **9**, 1902809.

26 C. Ding, D. Wang, D. Liu, H. Li, Y. Li, S. Hayase, T. Sogabe, T. Masuda, Y. Zhou, Y. Yao, Z. Zou, R. Wang and Q. Shen, Over 15% Efficiency PbS Quantum–Dot Solar Cells by Synergistic Effects of Three Interface Engineering: Reducing Nonradiative Recombination and Balancing Charge Carrier Extraction, *Adv. Energy Mater.*, 2022, **12**, 2201676.

27 A. H. Ip, S. M. Thon, S. Hoogland, O. Voznyy, D. Zhitomirsky, R. Debnath, L. Levina, L. R. Rollny, G. H. Carey, A. Fischer, K. W. Kemp, I. J. Kramer, Z. Ning, A. J. Labelle, K. W. Chou, A. Amassian and E. H. Sargent, Hybrid passivated colloidal quantum dot solids, *Nat. Nanotechnol.*, 2012, **7**, 577–582.

28 D. K. Ko, A. Maurano, S. K. Suh, D. Kim, G. W. Hwang, J. C. Grossman, V. Bulovic and M. G. Bawendi, Photovoltaic Performance of PbS Quantum Dots Treated with Metal Salts, *ACS Nano*, 2016, **10**, 3382–3388.

29 B. Sun, O. Voznyy, H. Tan, P. Stadler, M. Liu, G. Walters, A. H. Proppe, M. Liu, J. Fan, T. Zhuang, J. Li, M. Wei, J. Xu, Y. Kim, S. Hoogland and E. H. Sargent, Pseudohalide-Exchanged Quantum Dot Solids Achieve Record Quantum Efficiency in Infrared Photovoltaics, *Adv. Mater.*, 2017, **29**, 1700749.

30 Y. Kim, F. Che, J. W. Jo, J. Choi, F. P. Garcia de Arquer, O. Voznyy, B. Sun, J. Kim, M. J. Choi, R. Quintero-Bermudez, F. Fan, C. S. Tan, E. Bladt, G. Walters, A. H. Proppe, C. Zou, H. Yuan, S. Bals, J. Hofkens, M. B. J. Roeffaers, S. Hoogland and E. H. Sargent, A Facet-Specific Quantum Dot Passivation Strategy for Colloid Management and Efficient Infrared Photovoltaics, *Adv. Mater.*, 2019, **31**, e1805580.

31 J. Z. Fan, N. T. Andersen, M. Biondi, P. Todorovic, B. Sun, O. Ouellette, J. Abed, L. K. Sagar, M. J. Choi, S. Hoogland, F. P. G. de Arquer and E. H. Sargent, Mixed Lead Halide Passivation of Quantum Dots, *Adv. Mater.*, 2019, **31**, e1904304.

32 C. Ding, F. Liu, Y. Zhang, S. Hayase, T. Masuda, R. Wang, Y. Zhou, Y. Yao, Z. Zou and Q. Shen, Passivation Strategy of Reducing Both Electron and Hole Trap States for Achieving High-Efficiency PbS Quantum-Dot Solar Cells with Power Conversion Efficiency over 12%, *ACS Energy Lett.*, 2020, **5**, 3224–3236.

33 R. Wang, Y. Shang, P. Kanjanaboos, W. Zhou, Z. Ning and E. H. Sargent, Colloidal quantum dot ligand engineering for high performance solar cells, *Energy Environ. Sci.*, 2016, **9**, 1130–1143.

34 M. A. Boles, D. Ling, T. Hyeon and D. V. Talapin, The surface science of nanocrystals, *Nat. Mater.*, 2016, **15**, 141–153.

35 M. Liu, N. Yazdani, M. Yarema, M. Jansen, V. Wood and E. H. Sargent, Colloidal quantum dot electronics, *Nat. Electron.*, 2021, **4**, 548–558.

36 W. Wang, M. Zhang, Z. Pan, G. M. Biesold, S. Liang, H. Rao, Z. Lin and X. Zhong, Colloidal Inorganic Ligand-Capped Nanocrystals: Fundamentals, Status, and Insights into Advanced Functional Nanodevices, *Chem. Rev.*, 2022, **122**, 4091–4162.

37 M. Liu, O. Voznyy, R. Sabatini, F. P. Garcia de Arquer, R. Munir, A. H. Balawi, X. Lan, F. Fan, G. Walters, A. R. Kirmani, S. Hoogland, F. Laquai, A. Amassian and E. H. Sargent, Hybrid organic-inorganic inks flatten the energy landscape in colloidal quantum dot solids, *Nat. Mater.*, 2017, **16**, 258–263.

38 Y. Liu, H. Wu, G. Shi, Y. Li, Y. Gao, S. Fang, H. Tang, W. Chen, T. Ma, I. Khan, K. Wang, C. Wang, X. Li, Q. Shen, Z. Liu and W. Ma, Merging Passivation in Synthesis Enabling the Lowest Open-Circuit Voltage Loss for PbS Quantum Dot Solar Cells, *Adv. Mater.*, 2023, **35**, e2207293.

39 Y. Wang, Z. Liu, N. Huo, F. Li, M. Gu, X. Ling, Y. Zhang, K. Lu, L. Han, H. Fang, A. G. Shulga, Y. Xue, S. Zhou, F. Yang, X. Tang, J. Zheng, M. A. Loi, G. Konstantatos and W. Ma, Room-temperature direct synthesis of semi-conductive PbS nanocrystal inks for optoelectronic applications, *Nat. Commun.*, 2019, **10**, 5136.

40 F. Li, Y. Liu, G. Shi, W. Chen, R. Guo, D. Liu, Y. Zhang, Y. Wang, X. Meng, X. Zhang, Y. Lv, W. Deng, Q. Zhang, Y. Shi, Y. Chen, K. Wang, Q. Shen, Z. Liu, P. Müller-Buschbaum and W. Ma, Matrix Manipulation of Directly-Synthesized PbS Quantum Dot Inks Enabled by Coordination Engineering, *Adv. Funct. Mater.*, 2021, **31**, 2104457.

41 J. M. Luther, M. Law, Q. Song, C. L. Perkins, M. C. Beard and A. J. Nozik, Structural, optical, and electrical properties of self-assembled films of PbSe nanocrystals treated with 1, 2-ethanedithiol, *ACS Nano*, 2008, **2**, 271–280.

42 E. M. Sanehira, A. R. Marshall, J. A. Christians, S. P. Harvey, P. N. Ciesielski, L. M. Wheeler, P. Schulz, L. Y. Lin, M. C. Beard and J. M. Luther, Enhanced mobility CsPbI3 quantum dot arrays for record-efficiency, high-voltage photovoltaic cells, *Sci. Adv.*, 2017, **3**, eaao4204.

43 Y. Wang, K. Lu, L. Han, Z. Liu, G. Shi, H. Fang, S. Chen, T. Wu, F. Yang, M. Gu, S. Zhou, X. Ling, X. Tang, J. Zheng, M. A. Loi and W. Ma, In Situ Passivation for Efficient PbS Quantum Dot Solar Cells by Precursor Engineering, *Adv. Mater.*, 2018, **30**, 1704871.

44 G. Shi, H. Wang, Y. Zhang, C. Cheng, T. Zhai, B. Chen, X. Liu, R. Jono, X. Mao, Y. Liu, X. Zhang, X. Ling, Y. Zhang, X. Meng, Y. Chen, S. Duhm, L. Zhang, T. Li, L. Wang, S. Xiong, T. Sagawa, T. Kubo, H. Segawa, Q. Shen, Z. Liu and W. Ma, The effect of water on colloidal quantum dot solar cells, *Nat. Commun.*, 2021, **12**, 4381.

45 K. Lu, Y. Wang, Z. Liu, L. Han, G. Shi, H. Fang, J. Chen, X. Ye, S. Chen, F. Yang, A. G. Shulga, T. Wu, M. Gu, S. Zhou, J. Fan, M. A. Loi and W. Ma, High-Efficiency PbS Quantum-Dot Solar Cells with Greatly Simplified Fabrication Processing via "Solvent-Curing", *Adv. Mater.*, 2018, **30**, 1707572.